processes

MDPI

Article

Effective Desulfurization and Alumina Digestion of High-Sulfur Bauxite by New Roasting Process with Conveying Bed

Bo Zhao, Yanxin Chen * and Shaowu Jiu

College of Materials Science and Engineering, Xi'an University of Architecture and Technology, Xi'an 710055, China; 17792518719@xauat.edu.cn (B.Z.); jiushaowu@xauat.edu.cn (S.J.)
* Correspondence: chenyanxin@xauat.edu.cn; Tel.: +86-29-8220-2390

Abstract: A new roasting process with a conveying bed was constructed and used to remove sulfur of high-sulfur bauxite. Roasting temperature, phase transformation, microcrystal, specific surface area of high-sulfur bauxite, and the mechanism of the reaction during the roasting process were analyzed. The digestion properties of roasted bauxite were also investigated. The results showed that the sulfur in high-sulfur bauxite can be efficiently removed by roasting in the conveying bed at 520–720 °C for 2 s. Major reactions of high-sulfur bauxite during roasting were the dehydration of minerals, desulfurization of pyrite, sulfation of SO_2, and decomposition of sulfate. The rate of mineral dehydration reaction was significantly slower than that of the desulfurization reaction. The specific surface area of roasted ore greatly increased, and the microcrystal of Al-O mineral was refined, which was conducive to Al_2O_3 digestion. The mass fraction of sulfide sulfur in high-sulfur bauxite was reduced from 1.20% to 0.01%, and the relative digestibility of alumina reached more than 99% when roasting at 600 °C for 2 s. This paper provides revelations and instructions for the process development and application of high-sulfur bauxite.

Keywords: high-sulfur bauxite; roasting; conveying bed; desulfurization; activation; digestion

Citation: Zhao, B.; Chen, Y.; Jiu, S. Effective Desulfurization and Alumina Digestion of High-Sulfur Bauxite by New Roasting Process with Conveying Bed. *Processes* **2021**, *9*, 390. https://doi.org/10.3390/pr9020390

Academic Editor: Fabrizio Scala

Received: 8 February 2021
Accepted: 18 February 2021
Published: 20 February 2021

1. Introduction

Bauxite, the main raw material for aluminum production, is rapidly consumed with the development of modern industry. High-sulfur bauxite, a typical bauxite ore, has been estimated at 560 million tons in China [1], but it has not yet been effectively used. The mass fraction of sulfur in high sulfur bauxite is above 0.7%, and 90% of sulfur elements exist in the form of FeS_2. S_2^{2-} in high sulfur bauxite undergoes gradual transformation into $S_2O_3^{2-}$, SO_3^{2-}, and SO_4^{2-} during the Bayer process, which leads to adverse effects in production [2]. For example, it causes corrosion of steel equipment [3,4], an increase in alkali consumption [5], a reduction in heat transfer efficiency [6], and affects red mud sedimentation [7]. The sulfur content in raw material is required to be less than 0.4%wt in the Bayer alumina process, and desulfurization is a key factor in the utilization of high-sulfur bauxite. So, it is necessary to study the desulfurization of high-sulfur bauxite.

Major desulfurization methods of high-sulfur bauxite are floatation desulphurization, roasting desulphurization, and desulphurization in the digestion process. In the flotation desulfurization process, raw materials need to be ultra-finely ground, and then sulfonate traps are used to collect pyrite by inhibiting water seepage, which is very difficult to control [8–12]. Desulphurization in the digestion process involves the addition of a certain amount of oxygen or hydrogen peroxide as oxidant to oxidize sulfide sulfur into sulfate radical during the digestion of alumina under high temperature (150–350 °C) and high pressure (0.5–20 MPa) conditions. The desulfurization effect is greatly affected by the properties of raw materials and operating parameters, so the control of the production process is extremely difficult [13–16]. Roasting desulfurization is considered an ideal desulfurization method, as the pyrite in high-sulfur bauxite can be desulfurized by oxidative

calcination. Roasting desulfurization mainly includes direct roasting and additive roasting. Additionally, studies have examined dense-phase roasting, for instance, rotary kiln and fluidized beds, where high sulfur bauxite should be treated at 750°C minimum for at least 10 min [17–22]. Compared to dense-phase bed conditions, gas–solid contact area is larger, and heat/mass transfer rate and reaction rate are higher in the dilute phase conveying bed. Therefore, it is theoretically feasible to use a conveying bed for the roasting desulfurization of high-sulfur bauxite, but there has been no relevant research reported.

In this paper, the thermal reaction characteristics of high sulfur bauxite were analyzed by thermal-infrared spectroscopy. A semi-industrial conveying bed device was constructed for roasting desulfurization experiments of high sulfur bauxite, and the relationship between the desulfurization rate and temperature conditions was analyzed. The digestion properties of raw ore and roasted ore were analyzed and compared via digestion experiment. The mechanism of quality improvement of bauxite by conveying roasting was expounded via sulfur phase analysis, XRD, SEM, and a specific surface area test. Results confirmed that the new roasting process with a conveying bed was effective for roasting desulfurization of high-sulfur bauxite.

2. Experimental

2.1. Materials

High-sulfur bauxite from Chongqing province was used for roasting and digestion experiments. It was ground using a vertical roller mill and screened to under 100 μm. The average particle size of bauxite powder was determined as 48.5 μm. The main chemical composition of the bauxite is shown in Table 1 and was analyzed using chemical methods. The XRD pattern of high-sulfur bauxite is shown in Figure 1. Table 2 lists the mass fractions of the mineral composition.

Table 1. Chemical composition and loss on ignition of high-sulfur bauxite.

Compositions	Al_2O_3	SiO_2	Fe_2O_3	CaO	MgO	TiO_2	S_{Total}	S_2^{2-}	LOI
Contents (wt.%)	66.20	7.90	5.22	0.45	0.32	3.00	1.35	1.20	13.33

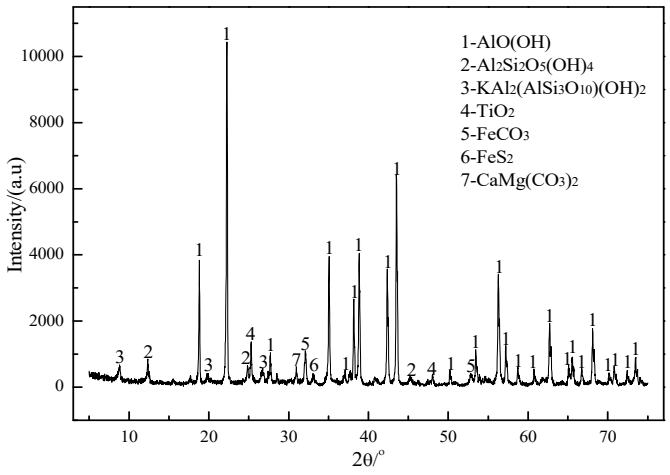

Figure 1. XRD pattern of high-sulfur bauxite.

Table 2. Mineral composition of high-sulfur bauxite.

Compositions	Diaspore AlO(OH)	Kaolinite $Al_2Si_2O_5(OH)_4$	Muscovite $KAl_2(AlSi_3O_{10})(OH)_2$	Pyrite FeS_2	Siderite $FeCO_3$	Anatase TiO_2	Dolomite $CaMg(CO_3)_2$
Contents (wt.%)	68.38	12.47	6.85	2.25	5.21	3.00	1.48

2.2. Thermal Infrared Spectroscopy Analysis

The test parameters of the thermal analyzer (NETZSCH 409PC STA, Selbu, Germany) and infrared spectrometer (Bruker FTIR-7600, Karlsruhe, Germany) were 90% N_2 + 10% O_2 atmosphere; a flow rate of 75 mL/min; heating rates of 5, 10, 15, and 20 °C/min; and a sample mass of 5.0 ± 0.5 mg. The type and flow rate of gas released during the roasting process were determined through infrared absorption analysis of the gas. Furthermore, the primary reactions and respective temperature regions were determined by TG, DTG, and FTIR analyses.

2.3. Experimental Facility and Method of Roasting

The semi-industrial test device consisted of a grinding system, suspension preheating system, external circulating conveying bed roasting furnace, suspension cooling system, flue gas cleaning system, and power system. An induced draft fan provided operating power for the whole system, which ran under negative pressure. Figure 2 shows the flow chart of the roasting experiment in the conveying system for high-sulfur bauxite.

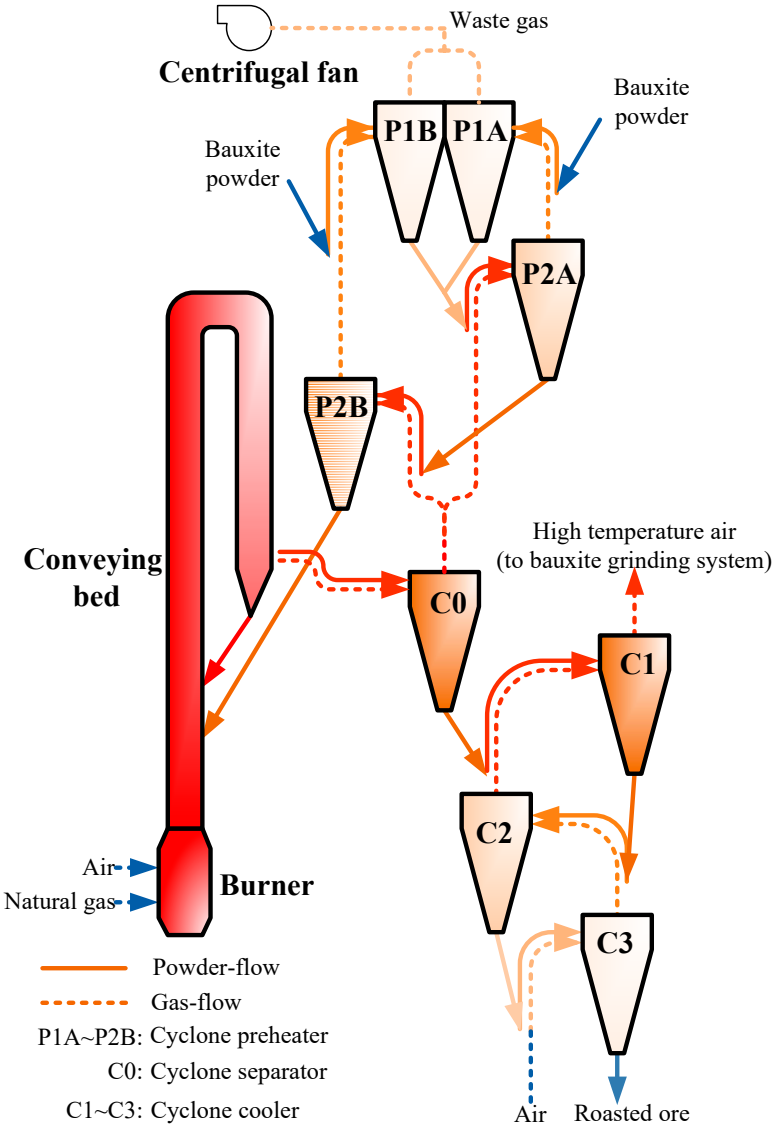

Figure 2. Flow chart of the roasting experiment in the conveying system for high-sulfur bauxite.

The material flow of the test unit was as follows: The feeding unit conveys high-sulfur bauxite powder to the heat exchange tube of cyclone preheater P1. P1 was a two-tube

cyclone and consisted of P1A and P1B. The heat exchange between the powder and updraft were instantly completed in the heat exchange tube, and gas and solid were then separated in the cylinder of P1 as the powder flowed into the heat exchange tube of P2A through the blanking tube of P1. The powder was preheated in the preheaters, which were in the order of P1, P2A, and P2B. Then, the powder flowed into the external circulating conveying bed, followed by dehydration and desulfurization under a high-temperature flue gas from the burner. Through a selective external circulating pathway, a certain amount of heavy or large particles were circulated by a cyclone separator to improve the thermal stability of the conveying bed, the reaction rate, and the treatment capacity per unit volume. Finally, two-phase gas–solid flowed into C0 to finish the gas–solid separation, and the roasted ore was cooled down in a three-stage cyclone cooling system, which consisted of C1, C2, and C3 in succession. The cooled low-temperature roasted ore was discharged into the product trough.

The gas flows of the test plant were as follows: high-temperature flue gas from the combustor flowed into conveying bed. After gas–solid separation in C0, flue gas was expelled into the preheating system through two divided parallel flows via the routes C0→P2A→P1A and C0→P2B→P1B, respectively. The two routes of flue gas converged at the outlet of P1 and flowed through the converging pipe, bag filter, centrifugal fan, and gas cleaning plant. At the same time, the cool gas flowed through C3, C2, and C1 in succession. After heat exchange with the high-temperature roasted ore, the temperature was increased to 300 °C, followed by flowing of cooling gas into the grinding drying system.

The length of the conveying bed reactor was 12 m, and the gas velocity in the reactor was measured at 6–6.3 m/s, so the apparent residence time of bauxite powders in the reactor was approx. 2 s. During the test, the system firstly required warming up and heat storage before the conveying bed reached a certain temperature. The initial feeding volume was 300 kg/h, and the furnace temperature achieved the expected set point through the adjustment of the natural gas flow rate, air flow of the whole system, air flow of the cooling system, and feed rate. When the system stabilized, the feed rate was 850 ± 10 kg/h. The roasting tests were run at 11 temperature spots between 520 and 720 °C. Roasted ore samples were collected every 10 min. At the end, the ore samples roasted at different temperatures were homogenized for further testing.

2.4. Experimental Facility and Method of Digestion

Digestion experiments were carried out in a steel bomb digester. According to the procedure requirements, ore pulp, which consisted of mother solution with a specific ratio for digestion, bauxite, and lime, was loaded into a 100 mL steel bomb and sealed. Subsequently, the steel bomb was installed in the rotatable shelf, then placed and stirred in a molten salt bath at the target temperature. When the scheduled time was reached, the steel bomb was removed and cooled in water. Finally, the digestion liquid and red mud were separated via vacuum filtration. Furthermore, the digestion liquid was analyzed for chemical components. The red mud was first washed and dried, then its chemical components and phase compositions were analyzed. The digestion ratio was calculated according to the silica–alumina ratio of bauxite and red mud.

The digestion effects of raw ore and roasted ore were tested via the relative digestion ratio of aluminum oxide and A/S in red mud through a series of digestion experiments at a temperature between 230 and 265 °C, digestion time of 50–70 min, caustic alkali concentration of 236 g/L, and 9% lime dosage. The relative digestion ratio of Al_2O_3 was calculated as follows:

$$\eta = \frac{(A/S)_{\text{ore}} - (A/S)_{\text{red mud}}}{(A/S)_{\text{ore}} - 1} \times 100\% \quad (1)$$

where η is the relative digestion ratio of aluminum oxide, $(A/S)_{\text{Ore}}$ is the mass ratio of Al_2O_3 and SiO_2 in bauxite ores, and $(A/S)_{\text{Red mud}}$ is the mass ratio of Al_2O_3 and SiO_2 in red mud.

2.5. Characterization

Powder X-ray diffraction (XRD) pattern, in the 2θ range of 5–75°, recording at a scan rate of 10°/min using a diffractometer (Rigaku D/MAX2200, Tokyo, Japan) with Cu Kα radiation was used for phase identification and analysis of the microlitic structure. The specific surface area was determined using the BET method. The morphological features of high-sulfur bauxite were studied using a scanning electron microscope (SEM) (Shimadzu SSX-550, Tokyo, Japan). The barium sulfate gravimetric method was adopted for the analysis of sulfur phase. A inductive coupled plasma emission spectrometer (ICP-OES) (PerkinElmer Optima 8000, Boston, MA, USA) was used for elemental analysis of digestion liquid and red mud.

3. Results and Discussion

3.1. Thermal Reaction Characteristics of High-Sulfur Bauxite

During the oxidation roasting process, various reactions occur, including the dehydration of hydrous mineral (e.g., diaspore and kaolinite) and the desulfurization of pyrite. Figure 3 shows TG/DTG curves of high-sulfur bauxite at different heating rates.

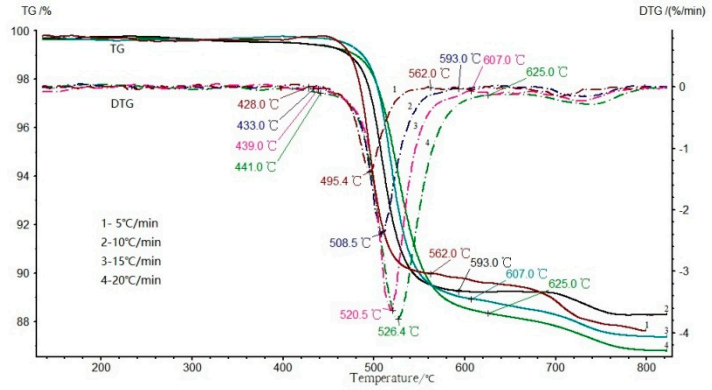

Figure 3. TG/DTG curves of high-sulfur bauxite at different heating rates.

As shown in Figure 3, the obvious weight loss of high sulfur bauxite begins at 420 °C and ends at about 790 °C. It can be seen from the DTG curve in Figure 2 that the decomposition process of high-sulfur bauxite consists of two stages. The first stage starts at about 420 °C and ends at 560–625 °C. The peak value of weight loss rate appears between 495.4 and 526.4 °C. In the second stage, the temperature range of weight loss is 670 –790 °C, and the peak temperature of weight loss is 705–735 °C. The initial temperature, peak temperature, and end temperature of the reaction shift to a high-temperature region with increasing heating rate.

Thermal infrared spectroscopy results show the relationship between the amount of gas produced and the respective temperature regions. Figure 4 shows a 3D infrared absorption spectrum under conditions of 15 °C/min. The absorption spectra of gases released at different temperatures (times) are presented in Figure 4. The infrared absorption spectra of gas released from high-sulfur bauxite mainly include O-H, S-O, and C-O groups. In accordance with the results of the mineral composition analysis of high-sulfur bauxite, it is determined that the gases corresponding to the three groups are H_2O (g), SO_2, and CO_2, respectively. The relationship between the temperature and gas flow of SO_2, H_2O, and CO_2 is shown in Figure 5, where the infrared absorption spectrum of a single component is converted and integrated using the Gram–Schmidt algorithm.

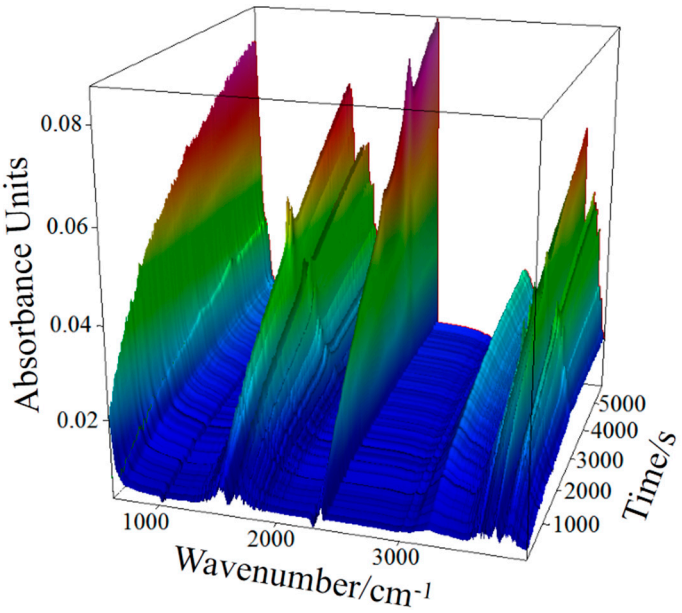

Figure 4. Infrared spectra of gas released from high–sulfur bauxite with a heating rate of 15 °C/min.

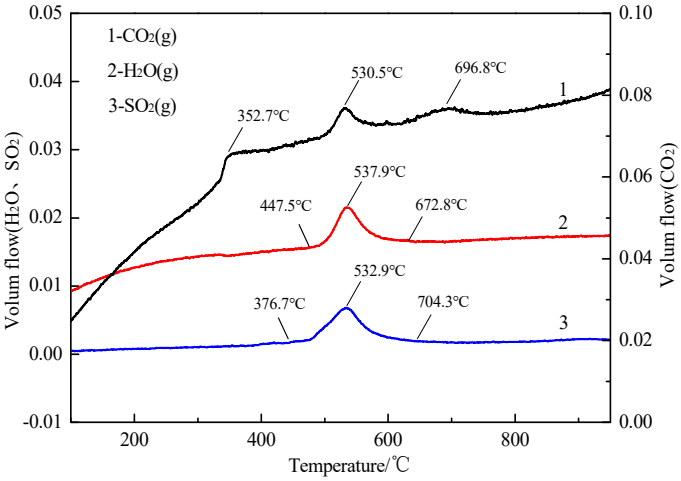

Figure 5. Relationship between the temperature and flow of three kinds of gas with a heating rate of 15 °C/min.

During the heating process at 15 °C/min, high-sulfur bauxite undergoes the oxidation of organic matter (around 352.7 °C), the dehydration of hydrous mineral (447.5–672.8 °C), the oxidation desulfurization of pyrite (367.7–704.3 °C), and the decomposition of carbonate minerals (around 530.5 and 696.8 °C), in which the decomposition temperature of siderite and dolomite is around 530.5 and 696.8 °C, respectively.

Furthermore, the temperature range of pyrite oxidation desulfurization, the dehydration of hydrous minerals such as diaspore and kaolinite, and siderite decomposition occur in an area of considerable overlap. Table 3 shows the possible reaction equations of bauxite and the standard reaction heat of each reaction at different temperatures, calculated using the Kirchhoff equation. The oxidation desulfurization of pyrite is a strong exothermic reaction, while the dehydration of hydrous minerals, such as diaspore and kaolinite, is an endothermic reaction. The desulfurization rate of pyrite and the dehydration of hydrous minerals determine the heat demand of the roasting process of high-sulfur bauxite, as determined by mineral composition (shown in Table 2).

Table 3. Reactions and heat of reaction of high-sulfur bauxite during the roasting process.

Chemical Reaction Equation	ΔH_T^{Θ}/(kJ/mol)		
	500 °C	550 °C	600 °C
$4FeS_2 + 11O_2(g) = 2Fe_2O_3 + 8SO_2(g)$	−3339.29	−3334.7	−3331.68
$2AlO(OH) = Al_2O_3 + H_2O(g)$	87.05	88.29	88.82
$Al_2Si_2O_5(OH)_4 = Al_2Si_2O_7 + 2H_2O(g)$	403.25	289.22	286.91
$4FeCO_3 + O_2(g) = 2Fe_2O_3 + 4CO_2(g)$	−67.84	−68.71	−69.72
$CaMg(CO_3)_2 = CaCO_3 + MgO + CO_2(g)$	—	—	—
$KAl_2(AlSi_3O_{10})\ (OH)_2 = KAl_2(AlSi_3O_{11}) + H_2O(g)$	—	—	—

Thermoanalysis results within the heating rate range of 5–20 °C/min show that with increasing heating rate, the temperature range of the dehydration and desulfurization reaction shifts to a high-temperature region; correspondingly, the temperature difference in the inflection point displays a slight increase. Hence, the temperature range of the reactions shifts to a high-temperature region with an increasing heating rate. Compared with the dense-phase bed, such as a rotary kiln or fluidized bed, the dilute-phase conveying bed exhibits a greater contact between gas and powders, and the reaction interface and transmission power in the boundary layer are larger. Furthermore, the heat and mass transfer coefficients are two magnitudes higher than those of the dense-phase bed. Heat transfer is completed quickly after powder flows into the conveying bed. Theoretical calculations show that 99.5% of the heat transfer between particles and gas is completed, and only in the initial region of the acceleration section in the whole powder dispersion process [23,24]. Therefore, the temperature corresponding to the maximum rate of the desulfurization and dehydration reactions of high-sulfur bauxite in the conveying bed is higher than that of thermoanalysis experiments, which were conducted in the stacking state.

3.2. Effect of Roasting Temperature on High-Sulfur Bauxite in Conveying Bed

The oxidation reaction of pyrite and the dehydration reaction of hydrous minerals may occur in the roasting process of high-sulfur bauxite, as well as "adsorption" and "desorption" between sulfur dioxide and powder particles. Therefore, in order to investigate the effect of the roasting process, the concepts of desulfurization rate (α), sulfate sulfur growth rate (β), and dehydration rate of hydrous minerals (γ) are introduced, where alumina is used as a fixed basis to calculate the above three rates. The three rates were calculated as follows:

$$\alpha = \left(1 - \frac{\omega(S_{sulfide})_R \times \omega(AO)_O}{\omega(S_{sulfide})_O \times \omega(AO)_R}\right) \times 100\%, \quad (2)$$

$$\beta = \left(\frac{\omega(S_{sulfate})_R \times \omega(AO)_O}{\omega(S_{sulfate})_O \times \omega(AO)_R} - 1\right) \times 100\%, \quad (3)$$

$$\gamma = \left(1 - \frac{\omega(H_2O)_R \times \omega(AO)_O}{\omega(H_2O)_O \times \omega(AO)_R}\right) \times 100\%. \quad (4)$$

α—Desulfurization rate of sulfide sulfur, %;
β—Increasing rate of sulfate sulfur, %;
γ—Dehydration rate of hydrous mineral, %;
$\omega(S_{sulfide})_R$—The mass fraction of sulfide sulfur in roasted ores, %;
$\omega(S_{sulfide})_O$—The mass fraction of sulfide sulfur in raw ores, %;
$\omega(AO)_R$—The mass fraction of Al_2O_3 in roasted ores, %;
$\omega(AO)_O$—The mass fraction of Al_2O_3 in raw ores, %;
$\omega(S_{sulfate})_R$—The mass fraction of sulfate sulfur in roasted ores, %;
$\omega(S_{sulfate})_O$—The mass fraction of sulfate sulfur in raw ores, %;
$\omega(H_2O)_R$—The mass fraction of combined water in roasted ores, %;
$\omega(H_2O)_O$—The mass fraction of combined water in raw ores, %.

Table 4 shows Al_2O_3, ignition loss, and sulfur phase analyses of ore roasted at various roasting temperatures.

Table 4. Analysis results of ore roasted at various roasting temperatures for approx. 2 s.

Temp.(°C)	ω_{Al2O3} (wt.%)	LOI (850 °C) (wt.%)	St (wt.%)	Sulfate Sulfur (wt.%)	Sulfide Sulfur (wt.%)
Raw ore	66.90	13.33	1.35	0.15	1.20
520	69.10	9.30	0.38	0.18	0.20
540	69.80	8.77	0.34	0.23	0.11
560	70.12	8.17	0.35	0.29	0.06
580	71.51	6.73	0.36	0.31	0.05
600	72.18	5.69	0.35	0.34	0.01
620	74.05	3.60	0.37	0.36	0.01
640	74.58	3.04	0.36	0.35	0.01
660	75.19	2.36	0.35	0.34	0.01
680	75.36	1.78	0.28	0.28	0.00
700	75.94	1.45	0.22	0.22	0.00
720	76.16	0.83	0.15	0.15	0.00

Figure 6 shows the trend of the relationship between the roasting temperature and the α, β, and γ of ore roasted at different roasting temperatures. Under the eleven selected roasting temperatures in the range of 520 to 720 °C, the rapid desulfurization of high-sulfur bauxite can be achieved in the conveying bed after approx. 2 s. Except for ore roasted at 520 °C, the total sulfur content of the other roasted ores is less than 0.37%, and the sulfide sulfur content of the roasted ore is below 0.11%.

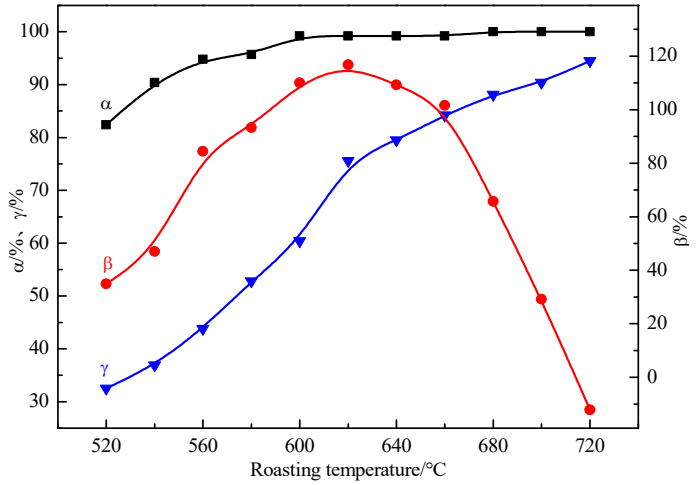

Figure 6. Trend of sulfur mass fraction and the desulfurization of roasted ore at various temperatures. α—desulfurization ratio of sulfide sulfur; β—increasing ratio of sulfate sulfur; γ—dehydration ratio.

As shown in Figure 6, the roasting temperature is positively correlated with α and γ. In the range of 520–620 °C, α and γ increase rapidly. At 520 °C, α reaches 80.4%, while γ is only 32.5%. At 600 °C, the sulfide sulfur content in the roasted ore decreases to 0.01%, and, compared with α 99.2%, γ is only 60.4%. Hence, the oxidation desulfurization reaction rate of FeS_2 is much higher than the dehydration reaction rate of hydrous minerals in the conveying bed. When the roasting temperature exceeds 620 °C, γ shows a significant decrease. At the temperature of 680 °C, the sulfide sulfur in roasted ore is completely removed, α reaches 100%, correspondingly, while γ is only 88.1%, which indicates that the thermal reaction rate of both reactions in the transport bed is quite different. Therefore, by controlling the roasting temperature in the conveying bed, pyrite can achieve a greater desulfurization rate, while the dehydration rates of hydrous minerals are relatively

small, meaning that the energy consumption for the roasting of high-sulfur bauxite can be maintained at a relatively low level, which reduces the overall energy consumption of the entire process.

Compared with dense-phase beds, such as rotary kilns, fluidized beds, and circulating fluidized beds, bauxite particles can be relatively dispersed in the gas phase in the dilute-phase conveying bed, the accumulation and mutual squeezing is greatly weakened, the effective contact area between particles and gas increases sharply, and the interface of heat and mass transfer expands, which is conducive to an increase in the heat and mass transfer rate. The fully developed turbulence of gas and powder exaggerate the Reynolds coefficient. Furthermore, the boundary layers of temperature and mass transfer become thinner, and the temperature gradient and concentration gradient become larger [25,26]. This results in the increased power of transmission which, in turn, improves the heat and mass transfer rate. Therefore, heat exchange and reaction between phases are realized within a few seconds.

The sulfate sulfur content initially shows an increasing tread followed by an obvious decrease, indicating that sulfate is formed in the roasting process of high-sulfur bauxite. β reaches the highest value of 116.8% at 620 °C and decreases beyond this temperature, which indicates that the sulfate sulfur is decomposed. Additionally, the total amount of sulfate sulfur in the roasted ore is lower than that of protogenetic sulfate in the raw ore when the value of β becomes negative at 720 °C.

The mechanism of sulfur dioxide absorption on ferric oxide was analyzed [27,28]. Fe_2O_3 has a positive influence on the absorption and fixing sulfur in the temperature range of 380–580 °C, where α-Fe_2O_3 displays an optimal effect of fixing sulfur, whose product is $Fe_2(SO_4)_3$; however, ferric sulfate decomposes into Fe_2O_3, SO_3, and SO_2 above 600 °C. During the roasting process of high-sulfur bauxite, Fe_2O_3 is generated via the desulfurization reaction of pyrite and the decomposition reaction of siderite, which combines with SO_2 to form ferric sulfate, promoting augmentation of the sulfate sulfur content in the roasted ore. Sulfate decomposition is a result of increased roasting temperature; at a roasting temperature of approx. 620 °C, the sulfate decomposition reaction rate increases and the growth rate of sulfate sulfur decreases. Therefore, when high-sulfur bauxite is roasted within a certain temperature range, three sulfur-related reaction processes take place: pyrite desulfurization, SO_2 adsorption to form sulfate, and sulfate decomposition.

Figure 7 shows the XRD patterns of ores roasted at different roasting temperatures. The intensity of the characteristic diffraction peaks of gibbsite, kaolinite, and siderite reduces rapidly with increasing roasting temperatures. The characteristic diffraction peaks of the three minerals basically disappear at 600 °C, indicating that the dehydration reaction of gibbsite and kaolinite and the decomposition reaction of siderite are basically complete. The characteristic diffraction peaks of pyrite overlap with those of hematite, which cannot be distinguished in an XRD comparison chart. Combined with the sulfide sulfur content in the roasted ore (Table 4), it can be determined that the oxidation reaction of pyrite finishes at 600 °C. As the roasting temperature increases, the heights of the characteristic diffraction peaks of dolomite and mica show only a slight change, which indicates that both minerals do not or rarely react when the roasting temperature is lower than 720 °C.

The desulfurization and dehydration reactions of high-sulfur bauxite are rapidly completed in the conveying bed, where diaspore and kaolinite are the main aluminous minerals. After dehydration, both minerals are transformed into α-Al_2O_3 and $Al_2O_3{\cdot}2SiO_2$, respectively, and the chemical activities of the reaction products directly influence the digestion effect of Al_2O_3. By comparing the XRD patterns of Figure 7 with the XRD patterns of Figure 1, the diffraction peaks of α-Al_2O_3 in the roasted ore (2θ = 35.3, 43.4, 57.4, and 68.2°) are wide and diffuse, and an increase in the sawtooth wave is observed, which indicates that diaspore dehydrates to form α-Al_2O_3 with fine grains or crystal defects. No obvious diffraction peak or "amorphous package" (2θ between 15 and 30°) of $Al_2O_3{\cdot}2SiO_2$ is detected in the roasted ore, and in the amorphous phase material, it is difficult to observe lattice vibration peaks; hence, metakaolinite is a disordered junction with a high degree of

amorphization in the roasted ore. At the dilute-phase conveying state, the dehydration reaction and roasted ore cooling occur within a few seconds. Flash roasting and flash cooling form α-Al_2O_3 and metakaolinite in the conveying system with a sharp temperature change and a great temperature gradient. Thus, it is difficult for α-Al_2O_3 to form a stable structure with regular crystal; the original aluminum octahedron structure of kaolinite is destroyed; and the observed sharp increase in amorphization leads to the dehydration of kaolinite into highly disordered amorphous metakaolinite.

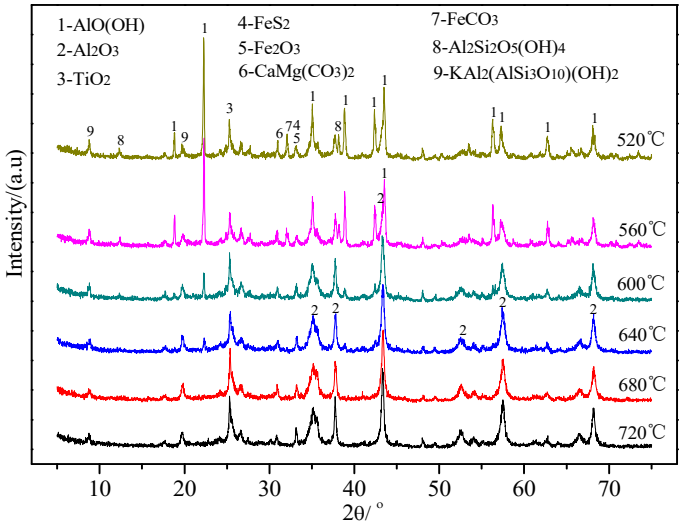

Figure 7. XRD patterns of ore roasted at different temperatures.

3.3. Digestion Properties of Roasted Ore

Reports have shown that there are many external factors that affect the digestion performance of bauxite, including digestion temperature, digestion time, lime addition, pulp concentration, caustic alkali concentration of mother liquor, and proportioning molecular ratio. The digestion temperature and time have a considerable influence on the industrial digestion process compared to other external factors. Therefore, only these two factors were taken as variables to investigate the variation in the relative digestion rate of alumina by alternating digestion temperature and time. Chemical reactions between roasted ore and alkali during digestion process mainly involve aluminous minerals and siliceous minerals. The reaction between α-Al_2O_3 in roasted ore and alkali are as follows:

$$Al_2O_3 + 2NaOH + aq \rightarrow 2NaAl(OH)_4 + aq \quad (5)$$

All aluminosilicate minerals are first decomposed into sodium aluminate and sodium silicate into the solution, and then both of them form hydrated sodium aluminosilicate. Taking metakaolinite as an example, the reaction is as follows:

$$Al_2O_3 \cdot 2SiO_2 + 6NaOH + aq \rightarrow 2NaAl(OH)_4 + 2Na_2[H_2SiO_4] + aq \quad (6)$$

$$2NaAl(OH)_4 + xNa_2[H_2SiO_4] + aq \rightarrow Na_2O \cdot Al_2O3 \cdot xSiO_2 \cdot nH_2O + 2xNaOH + aq \quad (7)$$

Figure 8 shows the influence of digestion temperature on the relative digestion rate of Al_2O_3, including raw ore and ore roasted at different roasting temperatures, under the conditions of 60 min digestion time, 9% lime addition, 236 g/L caustic concentration, and 1.50 ingredient molecular ratio. Figure 9 shows the influence of digestion time on the relative digestion rate of Al_2O_3 under the same conditions, except with 260 °C used as the digestion temperature.

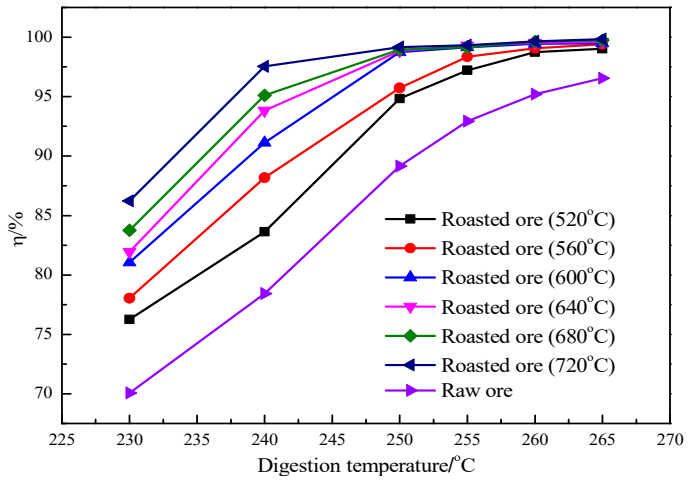

Figure 8. Effect of digestion temperature on the relative digestion rate under the conditions of 60 min digestion time, 9% lime addition, 236 g/L caustic concentration, and 1.50 ingredient molecular ratio.

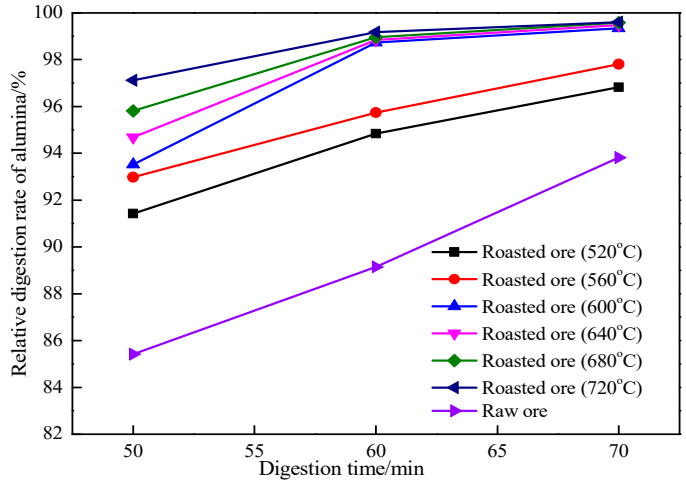

Figure 9. Effect of digestion time on the relative digestion rate under the conditions of 260 °C digestion temperature, 9% lime addition, 236 g/L caustic concentration, and 1.50 ingredient molecular ratio.

As shown in Figure 8, the digestion temperature significantly influences the relative digestion rate of Al_2O_3, especially that of raw ore, which is positively correlated to the digestion temperature. At the same digestion temperature, the relative digestion rate of roasted ore is higher than that of raw ore. Additionally, the roasting temperature increases with an increase in the relative digestion rate of the roasted ore, indicating that an elevated roasting temperature is conducive to the digestion of alumina in the roasted ore within a roasting temperature range of 520–720 °C and a digestion temperature range of 230–265 °C. Compared with the digestion temperature, the digestion time has no obvious influence on the digestion effect of the roasted ore. However, the relative digestion ratio of the raw ore is significantly affected by the digestion time.

When the digestion temperature is 250 °C and the digestion time is 60 min, the relative digestion rate of alumina in ore roasted at 600–720 °C reaches more than 99.0%, and the alumina in the roasted ore is basically completely dissolved. Using a higher digestion temperature or longer digestion time has no impact on the relative digestion rate of the ore roasted at a higher roasting temperature.

3.4. Activation Mechanism of Bauxite by Roasting in Conveying Bed

The obtained results show that the roasted ore has a better digestion performance than raw ore, as the relative digestion rate of alumina is greatly improved, and an enhanced digestion effect can be obtained under a relatively low digestion temperature and short digestion time.

The desulfurization and dehydration reactions of high-sulfur bauxite in the conveying bed are accomplished rapidly. Diaspore and kaolinite dehydrate are transformed into α-Al_2O_3 and $Al_2O_3 \cdot 2SiO_2$, respectively. The microcrystalline structures of diaspore in raw ore and alumina in roasted ore were analyzed by XRD, and the microcrystalline structure parameter D_{hkl} was calculated using the Debye–Scherrer formula in order to understand the changes that occur in the crystallite sizes of Al-O minerals after roasting in the conveying bed. The Debye–Scherrer formula was calculated as follows:

$$D_{hkl} = \frac{K\lambda}{\beta \cos\theta} \tag{8}$$

D_{hkl}—The size of microcrystals in the direction perpendicular to the crystal plane (hkl);
K—The parameter, 0.89;
λ—The wavelength of radiation, calculated according to the wavelength of $K_{\alpha 1}$, for the copper target, the value is 0.154056 nm;
θ—The half diffraction angle;
β—The broadening of diffraction peak, $\beta = \sqrt{B^2 - b^2}$;
B—The diffraction peak width (FWHM) of the sample;
b—The physical width of the instrument.

Figure 10 shows the trend of the α-Al_2O_3 crystallite size change with the variation in roasting temperature. The α-Al_2O_3 crystallite size perpendicular to planes 104, 113, 116, and 030 is at the nanometer level, and the maximum crystallite size is smaller than 24.5 nm, while the all-directional crystallite sizes of diaspore in the raw ore are greater than 100 nm. Hence, rapid roasting and dehydration in the conveying bed reduces the size of the crystallite of the Al-O mineral by one magnitude, which increases the microreaction interface. Moreover, the metakaolinite obtained through rapid roasting has a highly disordered amorphous structure. Under the combined action of these two aspects, the reactivity of the roasted ore during digestion greatly improves, which promotes the improvement of the digestion rate of alumina. The average size of α-Al_2O_3 crystallites increases from 14 nm at 520 °C to 20 nm at 720 °C, indicating that the use of a higher roasting temperature coarsens the α-Al_2O_3 microcrystal size, which has a negative impact on the digestion of alumina. However, the order of magnitude of crystallite sizes remains unchanged, making it difficult for them to have a large impact on the digestion of alumina.

Figure 11 shows the results for the specific surface area of raw ore and roasted ore determined by the multi-point BET method. The specific surface area of the raw ore is only 60 m^2/g, and that of the roasted ore increases significantly after rapid roasting in the conveying bed. The specific surface area range of the ore roasted below 560 °C only shows a small increase to 92 m^2/g, whereas above this temperature, it rapidly increases. The specific surface area of ore roasted at 600 °C with a test value of 128 m^2/g is more than double that of raw ore, whereas at 720 °C, it reaches 160 m^2/g. Due to the gas–solid heat transfer reaction being completed in seconds in the conveying bed, the temperature gradient and material concentration gradient between the gas and solid are large, and the heat and mass transfer rate is high, which allows the gas–solid reaction to be completed quickly. The SEM images of raw ore and roasted ore are shown in Figure 12. The roasting process had a significant influence on the microstructure of bauxite. In the SEM image of raw ore, a few cracks could be found on the particle surface, while many micropores were exposed on the surface of the roasted ore at 600 °C. In the condition of high transfer rate and thermal strength in the conveying bed, more pores and cracks should be produced by the dehydration and desulfurization reactions due to gas escaping, which increases the specific surface area of the roasted ore. In a certain temperature range below 720 °C, the specific

surface area of the roasted ore is positively correlated with temperature. Therefore, the liquid–solid reaction interface increases during the digesting process, which is beneficial to the relative digestion rate of alumina and the moderation of digestion conditions.

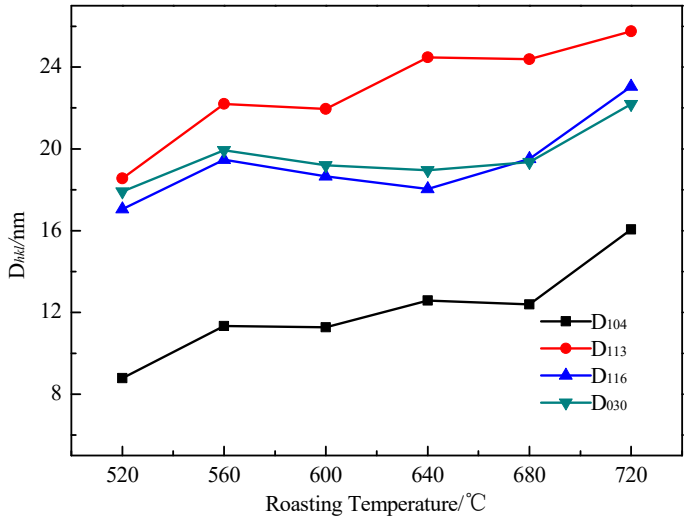

Figure 10. The trend of α-Al_2O_3 microcrystallite size change in ore roasted at varying temperatures.

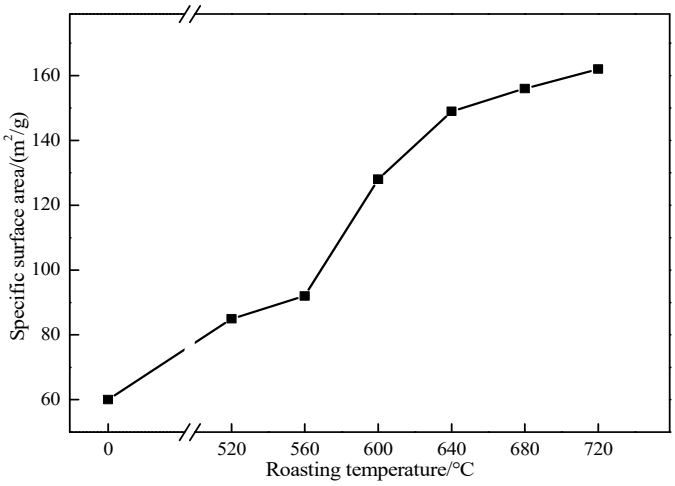

Figure 11. Specific surface area of bauxite at different temperatures calculated by BET.

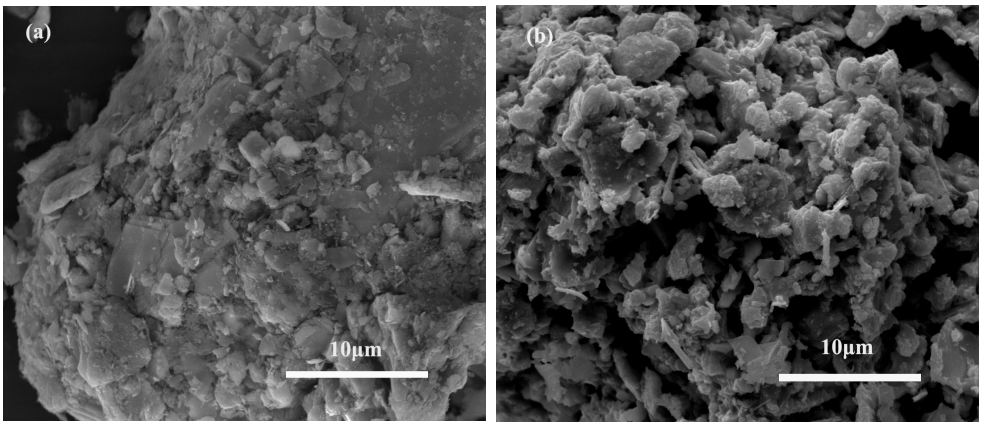

Figure 12. SEM images of bauxite: (**a**) raw ore; (**b**) ore roasted at 600 °C.

The rapid roasting of bauxite in the conveying bed reduces the crystallite sizes of Al-O minerals and increases the specific surface area of the roasted ore, which improves the microreaction interface of the subsequent liquid–solid reaction greatly. The roasted ore shows an enhanced digestion effect compared to the one obtained with the raw ore, greatly improving the processing performance of bauxite.

4. Conclusions

The proposed method is effective for the desulfurization of high-sulfur bauxite by the new conveying bed roasting process. The mass fraction of sulfide sulfur in the roasted ore can be reduced to 0.01%, and the relative digestibility of alumina can reach more than 99% at 600 °C for approx. 2 s.

The dehydration rate of high-sulfur bauxite and the sulfide sulfur desulfurization rate are positively correlated with temperature, and the overall progress of the dehydration reaction is obviously slower that of the desulfurization reaction. The roasting process involves the desulfurization of pyrite, a sulfation reaction between Fe_2O_3 and SO_2, and the decomposition reaction of sulfate. The increasing rate curve of sulfide sulfur is similar to a parabola, and the sulfate sulfur content reaches its maximum at 600 °C.

The Al-O crystal in the bauxite is refined; the specific surface area of the roasted ore greatly increases in the conveying bed; and the reaction interface expands during the digestion process, which is conducive to the digestion of alumina. Under the conditions of 260 °C digestion temperature, 60 min digestion time, 9% lime addition, 236 g/L caustic concentration, and 1.50 ingredient molecular ratio, the relative digestion rate of alumina in ore roasted at 600 °C reaches more than 99.0%, while it is only 89% in raw ore.

Author Contributions: Conceptualization, Y.C. and B.Z.; methodology, B.Z.; validation, Y.C., B.Z. and S.J.; formal analysis, Y.C.; investigation, B.Z. and S.J.; data curation and writing, B.Z.; visualization, S.J.; supervision, project administration and funding acquisition, Y.C. All authors have read and agreed to the published version of the manuscript.

Funding: This work was funded by the National Key R&D Program of China (No.), grant number 2016YFB0303400.

Institutional Review Board Statement: Not applicable.

Data Availability Statement: Not applicable.

Acknowledgments: The authors are grateful to the three anonymous reviewers for their constructive comments that greatly improved the manuscript.

Conflicts of Interest: The authors declare no conflict of interest.

References

1. Li, X.; Niu, F.; Liu, G.; Qi, T.; Zhou, Q.; Peng, Z. Effects of iron-containing phases on transformation of sulfur-bearing ions in sodium aluminate solution. *Trans. Nonferrous Met. Soc. China* **2017**, *27*, 908–916. [CrossRef]
2. Liu, Z.; Yan, H.; Ma, W.; Xiong, P. Sulfur Removal of High-Sulfur Bauxite. *Min. Met. Explor.* **2020**, *37*, 1617–1626. [CrossRef]
3. Yuan, J.; Chen, C.; Li, J.; Quan, B.; Lan, Y.; Wang, L.; Fu, H.; Gai, J. Initial Corrosion Behavior of 12Cr1MoV Steel in Thiosulfate-Containing Sodium Aluminate Solution. *Metals* **2020**, *10*, 1283. [CrossRef]
4. Xie, Q.; Chen, W.; Yang, Q. Corrosion behavior of four kinds of steels in sulfide-containing Bayer liquor. *J. Cent. South Univ. Sci. Technol.* **2014**, *45*, 2560–2565.
5. Bi, S. *Alumina Production Process*; Chemical Industry Press: Beijing, China, 2013; pp. 98–103.
6. Li, X.; Niu, F.; Tan, J.; Liu, G.; Qi, T.; Peng, Z.; Zhou, Q. Removal of S^{2-} ion from sodium aluminate solutions with sodium ferrite. *Trans. Nonferrous Met. Soc. China* **2016**, *26*, 1419–1424. [CrossRef]
7. Zhang, N.; Jiang, H.; Wu, X. Research on disposing of sulfur of high grade bauxite containing sulfur in Guizhou. *Light Met.* **2007**, *7*, 7–10. [CrossRef]
8. Blight, K.; Ralph, D.; Thurgate, S. Pyrite surfaces after bio-leaching: A mechanism for bio-oxidation. *Hydrometallurgy* **2000**, *58*, 227–237. [CrossRef]
9. Bulut, G.; Arslan, F.; Atak, S. Flotation behaviors of pyrites with different chemical compositions. *Min. Met. Explor.* **2004**, *21*, 86–92. [CrossRef]

10. Wang, C.; Zhang, Q.; Mao, S.; Qin, S. Effects of Fine Minerals on Pulp Rheology and the Flotation of Diaspore and Pyrite Mixed Ores. *Minerals* **2020**, *10*, 60. [CrossRef]
11. Wang, X.; Zhang, T.; Lv, G.; Bao, L.; Lv, B.; Jiang, X. Flotation process for desulfurization of high sulfur bauxite. *Chin. J. Rare Met.* **2009**, *33*, 728–732. [CrossRef]
12. Chai, W.; Huang, Y.; Peng, W.; Han, G.; Cao, Y.; Liu, J. Enhanced separation of pyrite from high-sulfur bauxite using 2-mercaptobenzimidazole as chelate collector: Flotation optimization and interaction mechanisms. *Miner. Eng.* **2018**, *129*, 93–101. [CrossRef]
13. Liu, Z.; Yan, H.; Ma, W.; Xie, K.; Xu, B.; Zheng, L. Digestion behavior and removal of sulfur in high-sulfur bauxite during bayer process. *Miner. Eng.* **2020**, *149*, 106237. [CrossRef]
14. Liu, Z.; Li, D.; Ma, W.; Yan, H.; Xie, K.; Zheng, L.; Li, P. Sulfur removal by adding aluminum in the bayer process of high-sulfur bauxite. *Miner. Eng.* **2018**, *119*, 76–81. [CrossRef]
15. Zhou, X.; Yin, J.; Chen, Y.; Xia, W.; Xiang, X.; Yuan, X. Simultaneous removal of sulfur and iron by the seed precipitation of digestion solution for high-sulfur bauxite. *Hydrometallurgy* **2018**, *181*, 7–15. [CrossRef]
16. Liu, Z.; Ma, W.; Yan, H.; Xie, K.; Li, D.; Zheng, L.; Li, P. Sulfur removal with active carbon supplementation in digestion process. *Hydrometallurgy* **2018**, *179*, 118–124. [CrossRef]
17. Hu, X.; Chen, W.; Xie, Q. Sulfur phase and sulfur removal in high sulfur-containing bauxite. *Trans. Nonferrous Met. Soc. China* **2011**, *21*, 1641–1647. [CrossRef]
18. Hu, X.; Chen, W.; Xie, Q. Desulfuration of high sulfur bauxite by oxidation roasting. *J. Cent. South Univ. Sci. Technol.* **2010**, *3*, 852–858.
19. Lu, D.; Lyu, G.; Zhang, T.; Zhang, W.; Xie, D.; Wang, Y.; Wang, L. Roasting Pretreatment-Low Temperature Digestion Method for Comprehensive Utilization of High-Sulfur Bauxite. *Light Met.* **2018**, 3–6. [CrossRef]
20. Jin, H.; Wu, F.; Li, J.; Chen, C.; Liu, H.; Yang, Q. Desulfurization of pyrite in high-sulfur bauxite with microwave roasting process. *J. Cent. South Univ. Sci. Technol.* **2020**, *51*, 2707–2717. [CrossRef]
21. Lou, Z.; Xiong, Y.; Feng, X.; Shan, W.; Zhai, Y. Study on the roasting and leaching behavior of high-sulfur bauxite using ammonium bisulfate. *Hydrometallurgy* **2016**, *165*, 306–311. [CrossRef]
22. Lv, G.; Zhang, T.; Bao, L.; Dou, Z.; Zhao, A.; Qu, H.; Ni, P. Roasting pretreatment of high-sulfur bauxite and digestion performance of roasted ore. *Chin. J. Nonferrous Met.* **2009**, *19*, 1684–1689. [CrossRef]
23. Xu, D. *Theory and Practice of Cement Suspended Preheating-Precalcining Technology*; Scientific and Technical Documentation Press: Beijing, China, 2002; pp. 81–99.
24. Li, Q.; Xu, D.; Chen, Y.; Yao, Y.; Sun, Z.; Ding, S. Decomposition of ammonium sulfate residue in a high solid/gas ratio suspension state with an industrial-scale reactor system (production line). *Particuology* **2015**, *22*, 107–113. [CrossRef]
25. Kwauk, M.; Li, J.H. *Manual of Fluidization*; Chemical Industry Press: Beijing, China, 2008; p. 228.
26. Li, J.H.; Kwauk, M. *Particle-Fluid Two-Phase Flow*; Metallurgical Industry Press: Beijing, China, 1994; pp. 60–66.
27. Wu, J.; Liu, S.; Han, Z. Mechanism of sulphur dioxide absorption on ferric oxide. *Sulphuric Acid Ind.* **1992**, *5*, 18–23.
28. Wu, J.; Liu, S. Kinetics of desulfurization using α-Fe_2O_3. *Acta Sci. Circumstantiae* **1990**, *10*, 49–57.